



# CHORUS

This is the accepted manuscript made available via CHORUS. The article has been published as:

## Determining individual phase response curves from aggregate population data

Dan Wilson and Jeff Moehlis

Phys. Rev. E **92**, 022902 — Published 3 August 2015

DOI: [10.1103/PhysRevE.92.022902](https://doi.org/10.1103/PhysRevE.92.022902)

# Determining Individual Phase Response Curves from Aggregate Population Data

Dan Wilson and Jeff Moehlis

*Department of Mechanical Engineering, University of California, Santa Barbara, CA 93106, USA*

Phase reduction is an invaluable technique for investigating the dynamics of nonlinear limit cycle oscillators. Central to the implementation of phase reduction is the ability to calculate phase response curves (PRCs), which describe an oscillator's response to an external perturbation. Current experimental techniques for inferring PRCs require data from individual oscillators, which can be impractical to obtain when the oscillator is part of a much larger population. Here we present a simple yet novel methodology to calculate PRCs of individual oscillators using an aggregate signal from a large homogeneous population. This methodology is shown to be accurate in the presence of inter-oscillator coupling and noise and can also provide a good estimate of an average PRC of a heterogeneous population. We also find that standard experimental techniques for PRC measurement can produce misleading results when applied to aggregate population data.

PACS numbers: 87.19.lj, 02.30.Zz, 02.30.Nw

## I. INTRODUCTION

Collective oscillation in populations of limit cycle oscillators is a widely observed phenomenon in nonlinear biological sciences [1], [2], [3], [4]. To understand the collective behavior of these systems, it is often useful to reduce the dynamics of the constituent oscillators through phase reduction [5], [4], [6], so that each oscillator obeys an equation of the form

$$\dot{\theta} = \omega + Z(\theta)u(t), \quad (1)$$

where the phase  $\theta \in [0, 2\pi)$  describes an oscillator's position in the basin of attraction of a limit cycle,  $\omega$  is the natural frequency so that the natural period  $T = 2\pi/\omega$ , and  $Z(\theta)$  is the infinitesimal phase response curve (PRC) which captures the oscillator's response to a small perturbation,  $u(t)$ . We note that (1) can be appended to include additional terms such as noise and coupling in a population. Phase reduction has been applied fruitfully to many applications to both understand and control populations of phase oscillators [7], [8], [5], [9], [10], [11].

Essential to the understanding of these oscillatory group dynamics is the ability to accurately compute PRCs, which for systems *in silico* has been rendered nearly trivial with modern computing algorithms and software [12], [13], [14]. For living systems, however, the model equations are not usually known, and calculating PRCs is more difficult. For example, accurately measuring PRCs in neurons using the "direct method" [3], [15], [16] requires current to be injected through a dynamic clamp, piercing the cell membrane and ultimately killing the neuron in the process. While recordings from individual neurons can be difficult to measure, readings from populations of neurons are readily available in experimental neurology, for example, in the form of the local field potential, which represents a filtered sum of current traveling across the cell membranes of a population of nearby cells [17].

When it is difficult or impractical to obtain data from an individual oscillator for calculating its PRC, it may be more convenient to study the macroscopic behavior of the population. To this end, [18], [19], [20] and [21] investigate the relationship between the phase sensitivity of a individual limit cycle oscillators and the phase sensitivity of their collective oscillation which arises due to coupling. Also, [22] derived a method to calculate phase response curves for the collective oscillations in excitable systems. These methods, however, require that the population oscillation approaches a limit cycle, which can be a relatively strict assumption.

In this work, we propose a methodology that can calculate individual PRCs using only an aggregate signal produced by the collective oscillation of a population of homogeneous oscillators which does not require the collective oscillation itself to approach a limit cycle. While this methodology is developed for a homogeneous uncoupled population, we find that it is robust to both heterogeneity in the individual oscillators, uncertainty in the signal being measured, and terms which are unaccounted for such as noise and coupling. Furthermore, we find that the standard methods used to calculate PRCs in individual oscillators can produce misleading

results when directly applied to populations of oscillators. This methodology could make control strategies such as [23], [24], and [25] more feasible for *in vivo* testing when the individual elements in the population are difficult to observe.

## II. NUMERICAL PROCEDURE

To begin, consider a large group of  $N$  identical, uncoupled phase oscillators [1], [3]:

$$\dot{\theta}_i = \omega + Z(\theta_i)\psi\delta(t - \tau) + \mathcal{O}(\epsilon). \quad (2)$$

Here,  $\theta_i \in [0, 2\pi)$  is the phase of oscillator  $i = 1, 2, \dots, N$ ,  $Z(\theta)$  is the PRC, and  $\psi\delta(t - \tau)$  is a  $\delta$ -function impulse of strength  $\psi \in \mathbb{R}$  applied identically to each oscillator. In (2), we allow for unknown but small  $\mathcal{O}(\epsilon)$  perturbations. Suppose we have no information about any individual oscillators, but that each cell emits a phase dependent signal  $s(\theta)$  so that the aggregate signal

$$\bar{s}(t) = \frac{1}{N} \sum_{i=1}^N s(\theta_i(t)) \quad (3)$$

can be measured from the distribution.

When  $N$  is very large, we can characterize the distribution of phase oscillators with a probability density  $\rho(t, \theta)$  [26]:

$$\begin{aligned} \frac{\partial \rho}{\partial t} &= -\frac{\partial}{\partial \theta}[(\omega + Z(\theta)\psi\delta(t - \tau) + \mathcal{O}(\epsilon))\rho(t, \theta)] \\ &= -\omega\rho_\theta - \psi[Z(\theta)\rho_\theta + Z_\theta(\theta)\rho]\delta(t - \tau) + \mathcal{O}(\epsilon). \end{aligned} \quad (4)$$

Equation (4) implicitly assumes that the first derivative of  $\rho$  is  $\mathcal{O}(1)$  and the  $\mathcal{O}(\epsilon)$  terms are small. In the absence of  $\delta$ -function forcing and  $\mathcal{O}(\epsilon)$  terms, equation (4) admits periodic traveling wave solutions. This knowledge can be exploited to calculate the probability density immediately prior to and after a  $\delta$ -function pulse, which will be necessary for calculating phase response curves.

### A. Estimating the Population Distribution from the Aggregate Signal

Consider the one dimensional Fokker-Planck equation (4). For all times  $t \neq \tau$ , we asymptotically expand the solution of (4) in orders of  $\epsilon$  as  $\rho(t, \theta) = \rho^{(0)}(t, \theta) + \epsilon\rho^{(1)}(t, \theta) + \epsilon^2\rho^{(2)}(t, \theta) \dots$ , and find that,  $\frac{\partial}{\partial t}\rho^{(0)}(t, \theta) = -\omega\rho_\theta$  so that

$$\rho(t, \theta) = \rho_o(\theta - \omega t) + \epsilon\rho^{(1)}(t, \theta) + \mathcal{O}(\epsilon^2), \quad (5)$$

where  $\rho_o(\theta) = \rho(0, \theta)$ . For the moment, we will neglect the  $\mathcal{O}(\epsilon)$  and  $\mathcal{O}(\epsilon^2)$  terms so that

$$\bar{s}(t) = \frac{1}{2\pi} \int_0^{2\pi} \rho_o(\theta - \omega t)s(\theta)d\theta. \quad (6)$$

If we take  $\Delta\theta$  small enough, errors in the following approximation of (6) are negligible:

$$\bar{s}(\Delta tm) = \frac{1}{M} \sum_{j=1}^M \rho_o(\Delta\theta j - \omega m\Delta t)s(\Delta\theta j). \quad (7)$$

Assuming that we have carefully chosen  $\Delta\theta$  so that the sampling rate  $\Delta t = \Delta\theta/\omega$ , letting  $\bar{s}(\Delta tm) \rightarrow \bar{s}_m$ ,  $\rho_o(\Delta\theta m) \rightarrow \rho_{o_m}$ , and  $s(\Delta\theta m) \rightarrow s_m$ , we may write

$$\bar{s}_m = \frac{1}{M} \sum_{j=1}^M \rho_{o_{j-m}} s_j, \quad (8)$$

where  $\bar{s}$ ,  $s$ , and  $\rho_o$  now represent vectors in  $\mathbb{R}^M$  and  $M = 2\pi/\Delta\theta = T/\Delta t$ . Defining  $\bar{s}_x^c = \bar{s}_{M-x}$  and  $s_x^c = s_{M-x}$ , and letting  $m = M - k$  and  $j = g + M - k$ , we can manipulate the previous equation to give

$$\begin{aligned}\bar{s}_{M-m}^c &= \frac{1}{M} \sum_{j=1}^M \rho_{o_{j-m}} s_{M-j}^c, \\ \bar{s}_k^c &= \frac{1}{M} \sum_{j=1}^M \rho_{o_{j-M+k}} s_{M-j}^c, \\ \bar{s}_k^c &= \frac{1}{M} \sum_{g=1}^M \rho_{o_g} s_{k-g}^c, \\ \implies \bar{s}^c &= \frac{1}{M} (\rho_o * s^c)\end{aligned}\tag{9}$$

where  $*$  is the convolution operator. Note here that we are using periodicity in  $s$  so that, for example, if  $k - g \leq 0$ ,  $s_{k-g}^c = s_{M+k-g}^c$ . Thus, letting  $\mathcal{F}$  represent the discrete Fourier transform,  $\rho_o$  can be found using the relation

$$\frac{\rho_o}{M} = \mathcal{F}^{-1} \left( \frac{\mathcal{F}(\bar{s}^c)}{\mathcal{F}(s^c)} \right).\tag{10}$$

If we account for the leading order  $\epsilon$  terms in equation (5) we can rewrite (8) as

$$\begin{aligned}\bar{s}_m &= \frac{1}{M} \sum_{j=1}^M (\rho_{o_{j-m}} + \epsilon \rho_{j,m}^{(1)}) s_j \\ &= \frac{1}{M} \sum_{j=1}^M \rho_{o_{j-m}} s_j + \frac{1}{M} \sum_{j=1}^M \epsilon \rho_{j,m}^{(1)} s_j,\end{aligned}\tag{11}$$

where  $\rho_{j,m}^{(1)} \in \mathbb{R}^M$  is a vector representing the discretized distribution  $\rho^{(1)}(m\Delta t, j\Delta\theta)$ . With the same manipulations we used in equation (9), we arrive at the relation

$$\bar{s}_k^c = \frac{1}{M} \sum_{g=1}^M \rho_{o_g} s_{k-g}^c + \frac{\epsilon}{M} \sum_{j=1}^M (\rho_{j,M-k}^{(1)} s_{M-j}^c),\tag{12}$$

and therefore,

$$\frac{\mathcal{F}(\rho_o)}{M} = \frac{\mathcal{F}(\bar{s}^c)}{\mathcal{F}(s^c)} - \frac{\epsilon \mathcal{F}(W)}{M \mathcal{F}(s^c)},\tag{13}$$

where  $W_k = \frac{1}{M} \sum_{j=1}^M (\rho_{j,M-k}^{(1)} s_{M-j}^c)$ . Thus, the term  $\frac{\epsilon \mathcal{F}(W)}{M \mathcal{F}(s^c)}$  adds order  $\epsilon$  error to each of the Fourier coefficients. Generally,  $\mathcal{F}(s^c)$  will be close to zero for contributions from higher order Fourier coefficients, which can amplify error in calculating higher order modes of the distribution  $\rho_o$ . For this reason, we truncate the calculated distribution in the main text to include only the lowest order Fourier modes.

## B. Connecting the Fokker-Planck Phase Response Functional to the Individual Neuron Phase Response Curve

Again, neglecting  $\mathcal{O}(\epsilon)$  terms, (4) admits traveling wave solutions allowing us to study its solution in terms of a group phase  $\Theta$ , defined here so that  $\Theta \in [0, 2\pi)$  and  $\kappa \cos(\theta - \Theta)$  is the first Fourier mode of the distribution  $\rho(t, \theta)$ . With this definition of group phase, we may view the network (4) itself as a phase oscillator which evolves according to

$$\dot{\Theta} = \omega + \left\langle G(\theta, \Theta), -\psi[Z(\theta)\rho_\theta + Z_\theta(\theta)\rho]\delta(t - \tau) + \mathcal{O}(\epsilon) \right\rangle,\tag{14}$$

where  $G(\theta, \Theta)$  is the group phase response functional, and  $\langle \cdot, \cdot \rangle$  is the  $L^2$  inner product. As we show in Appendix A by using techniques similar to those in [22],  $G(\theta, \Theta) = \frac{\sin(\theta - \Theta)}{\kappa\pi}$ , where  $\kappa$  is the magnitude of the first Fourier mode of  $\rho(t, \theta)$ . Therefore, the change in group phase  $\Delta\Theta$  due to the  $\delta$ -function impulse is

$$\Delta\Theta = -\frac{\psi}{\kappa\pi} \langle \sin(\theta - \Theta), Z(\theta)\rho_\theta + Z_\theta(\theta)\rho \rangle. \quad (15)$$

Because  $\rho(t, \theta)$  can be determined by through measurements of  $\bar{s}(t)$  using (10), and  $\Delta\theta$  is defined so that it can be found with knowledge of  $\rho(t, \theta)$ , equation (15) allows us to use these observable values in order to infer the phase response curve of the individual oscillators. It should be noted that if  $\rho(t, \theta) = \delta(\theta - \theta_o)$  equation (15) reduces to  $\Delta\Theta(\theta_o)/\psi = Z(\theta_o)$ , i.e. the PRC can be measured precisely with a direct method. However, when  $\rho$  is not a  $\delta$ -function, we will find that simply using the direct method to calculate PRCs can yield misleading and incorrect results. To proceed, we define two new functions

$$\begin{aligned} \rho_f(t, \theta) &= \rho(t, \theta) - \sum_{k=q+1}^{\infty} B_{\rho,k} \sin(k(\phi_{\rho,k} - \theta)), \\ Z_f(\theta) &= Z(\theta) - \sum_{k=q+1}^{\infty} B_{Z,k} \sin(k(\phi_{Z,k} - \theta)), \end{aligned} \quad (16)$$

where  $B_{\rho,k} \sin(k(\phi_{\rho,k} - \theta))$  and  $B_{Z,k} \sin(k(\phi_{Z,k} - \theta))$  represent the  $k^{\text{th}}$  Fourier modes of  $\rho(t, \theta)$  and  $Z(\theta)$ , respectively. If we take  $q$  large enough so that  $|\rho - \rho_f|$ ,  $|Z - Z_f|$  and their first derivatives with respect to  $\theta$  are small, it is reasonable to assume that

$$\Delta\Theta = -\frac{\psi}{\kappa\pi} \langle \sin(\theta - \Theta), Z_f \rho'_f + Z'_f \rho_f \rangle + \mathcal{O}(\epsilon), \quad (17)$$

where  $' \equiv \partial/\partial\theta$ . Here we have assumed that using the truncated terms for  $\rho_f$  and  $Z_f$  in (15) only lead to  $\mathcal{O}(\epsilon)$  errors in the inner product. The Fourier coefficients of the phase distributions immediately preceding and following a  $\delta$ -function pulse,  $\rho(\tau^-, \theta)$ , and  $\rho(\tau^+, \theta)$ , respectively, can be determined from (10). For instance,  $\rho(\tau^-, \theta)$  can be found taking  $\bar{s}^c = [\bar{s}(\tau - T/M), \bar{s}(\tau - 2T/M), \dots, \bar{s}(\tau - T)]$ , with  $s^c = [s(2\pi(1 - \frac{1}{M})), s(2\pi(1 - \frac{2}{M})), \dots, s(0)]$ . We can then use the recordings after the  $\delta$ -function stimulus to calculate  $\rho(\tau^+, t)$  and hence calculate  $\Delta\Theta$ . Finally, we are in a position to present a strategy to obtain  $Z(\theta)$ :

1. Record  $\bar{s}(t)$  on the interval  $t \in [\tau - T, \tau + T]$ , where a  $\delta$ -function pulse is given at  $t = \tau$ .
2. Repeat  $p$  times where  $p \geq 2q + 1$ . Recall that  $q$  determines the number of Fourier modes of  $Z$  that we wish to estimate.
3. Using the data from steps 1 and 2, construct the matrix  $A \in \mathbb{R}^{p \times (2q+1)}$  and vector  $b \in \mathbb{R}^p$ , as defined below.
4. Solve for the best fit of the Fourier coefficients  $c = A^\dagger b$ , where  $^\dagger$  denotes the pseudoinverse [27].

Here  $b_i$  corresponds to the  $i^{\text{th}}$  measurement of  $\Delta\Theta$ . For the  $k^{\text{th}}$  set of recordings, we use the first  $q$  modes of  $\rho(\tau^-, \theta)$  to construct  $\rho_{f,k}$ . Using the notation  $Z_f(\theta) = c_1 + \sum_{v=1}^q c_{2v} \sin(v\theta) + \sum_{w=1}^q c_{2w+1} \cos(w\theta)$ , we can rewrite equation (17) as:

$$\begin{aligned} [A_{k,1}, A_{k,2}, \dots, A_{k,2q+1}] [c_1, c_2, \dots, c_{2q+1}]^T &= b_k + \mathcal{O}(\epsilon) \\ A_{k,1} &= -\frac{\psi}{\kappa\pi} \langle \sin(\theta - \Theta), \rho'_{f,k} \rangle \\ A_{k,2v} &= -\frac{\psi}{\kappa\pi} \langle \sin(\theta - \Theta), \sin(v\theta)\rho'_{f,k} + v \cos(v\theta)\rho_{f,k} \rangle \\ A_{k,2w+1} &= -\frac{\psi}{\kappa\pi} \langle \sin(\theta - \Theta), \cos(w\theta)\rho'_{f,k} - w \sin(w\theta)\rho_{f,k} \rangle. \end{aligned} \quad (18)$$

In the equation above, we calculate  $\Theta$  from  $\rho(\tau^-, \theta)$ . An estimate of the Fourier coefficients of  $Z$  can then be determined by taking  $A^\dagger b$ . We note that the  $\mathcal{O}(\epsilon)$  terms from (18) will not cause the estimate of the true

Fourier coefficients of  $Z$  to deviate by more than  $\mathcal{O}(\epsilon)$  because  $A$  does not depend on  $\epsilon$ , and  $\|A^\dagger\|$ , while potentially large, will be bounded if we take enough independent measurements so that  $A$  has full rank.

As a final note, without the unknown  $\mathcal{O}(\epsilon)$  terms from equation (2), the only source of error in this procedure results from the truncations of  $Z$  and  $\rho$  in (16). When we include these small terms, as we show in Appendix B, they contribute an additional  $\mathcal{O}(\epsilon)$  error in the calculation of the Fourier coefficients of  $Z(\theta)$ .

### III. NUMERICAL RESULTS FOR A NETWORK OF OSCILLATORY NEURONS

We now test the utility of this method on a model which exhibits periodic neural spiking behavior. First consider a model of  $N = 1000$  periodically spiking thalamic neurons [28]:

$$\begin{aligned}
C\dot{V}_i &= -I_L(V_i) - I_{Na}(V_i, h_i) - I_K(V_i, h_i) \\
&\quad - I_T(V_i, r_i) + I_{i,SM} + \zeta_i u(t) + D\eta_i(t) + \frac{\alpha_c}{N} \sum_{j=1}^N (V_j - V_i), \\
\dot{h}_i &= (h_\infty(V_i) - h_i)/\tau_h(V_i), \\
\dot{r}_i &= (r_\infty(V_i) - r_i)/\tau_r(V_i), \quad i = 1, \dots, N.
\end{aligned} \tag{19}$$

Here,  $V_i$ ,  $h_i$ , and  $r_i$  are transmembrane voltage and gating variables for neuron  $i$ ,  $u(t) = I(t)/C$  represents a control input common to all neurons,  $\zeta_i$  is a constant representing the proximity to the stimulus electrode,  $I_{i,SM}$  represents a baseline current chosen so that each neuron fires periodically,  $\eta_i(t) = \mathcal{N}(0, 1)$  is i.i.d. noise with zero mean and variance 1,  $D$  and  $\alpha_c$  are constants determining the strength of the noise and electrotonic coupling [29], respectively, and all other functions and parameters are given in [28]. We note that this network could be generalized to include, for instance, chemical synaptic coupling with more complicated coupling structures. In our first example, we take the network to be homogeneous with  $I_{i,SM} = 5\mu\text{A}/\text{cm}^2$  and  $\zeta_i = 1$  for all  $i$ . We also set  $D = \alpha_c = 0$  so that the distribution evolves according to (4) with no  $\mathcal{O}(\epsilon)$  terms. When  $u(t) \equiv 0$ , each neuron settles to the same stable limit cycle, and we take  $s(\theta)$  to be the transmembrane voltage along this cycle, shown in panel A of Figure 1. We take  $p = 70$  measurements taking  $u(t)$  to approximate a  $\delta$ -function with  $\psi = 0.025$  using the methodology described above. Panel B shows an example of  $\bar{s}(t)$  centered at  $t = \tau$ , the time at which the perturbation is applied. Panel C shows raw measurements of  $\Delta\Theta/\psi$  plotted against the phase that the stimulus was applied, similar to how PRCs are typically measured in single neuron recordings [15], and panel D gives the estimated PRC using the methodology detailed above with  $M = 1000$  and  $q = 4$  (black line) with the exact PRC (grey line) measured using XPPAUT [12]. Note that while there is a strong, seemingly sinusoidal, correlation between  $\Theta$  and  $\Delta\Theta$ , this does not capture the phase response properties of the individual neurons.

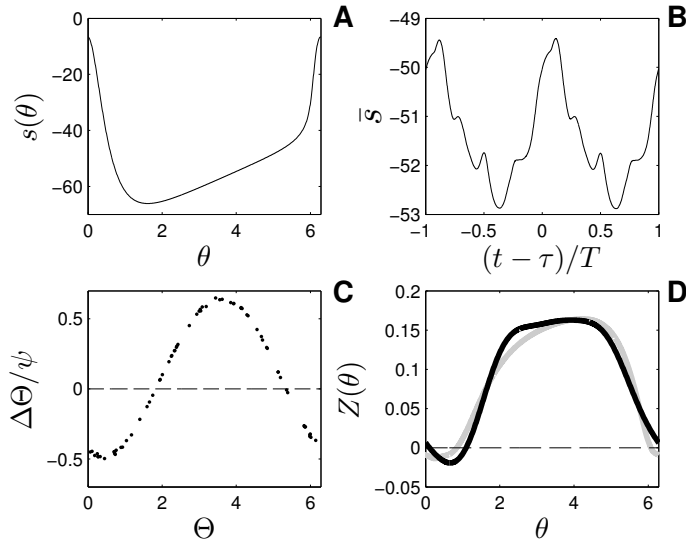


FIG. 1. Panel A shows the transmembrane voltage as a function of  $\theta$  on the limit cycle, which we take to be  $s(\theta)$ . Panel B shows an example measurement of  $\bar{s}$  for a perturbation at  $t = \tau$ . Panel C shows a strong, potentially misleading correlation between the initial phase and  $\Delta\Theta$  which does not accurately reflect the true PRC in Panel D. The PRC calculated from the data using the methods of Section II is shown in black in Panel D with the true PRC in grey.

### A. Including Heterogeneity, Coupling and Noise

In the derivation of the phase response calculation methodology from Section II, we assume that the phase response curves and natural frequencies of each oscillator are identical. In all but the simplest applications, this is an overly restrictive assumption. Here, we provide numerical evidence that in a heterogeneous network, the proposed methodology can accurately estimate the average phase response curve of the system. Furthermore, while we show in Appendix B that this methodology is guaranteed to be accurate when each oscillator is subject to small unknown external perturbations (e.g. noise and coupling), we find that this methodology can still yield accurate results when external perturbations are large.

To include heterogeneity in the neural network (19), we draw the parameters  $I_{SM}$ ,  $\zeta$  and the leak current conductance, ( $g_L$  from [28]) in (19) from normal distributions, with histograms for the chosen values shown in Figure 2. For this choice of parameters, both the PRCs and the natural periods of each neuron in the population are no longer identical. We take  $s(\theta)$  to be voltage along the limit cycle, averaged over each neuron which gives a similar  $s(\theta)$  to what was used in the homogeneous population example (we note that this calculation of  $s(\theta)$  would not be feasible in a real experiment, and provide a discussion about robustness with respect to the choice of  $s(\theta)$  in the next section).

In order to apply the numerical procedure from Section IIB to the heterogeneous population, we need to determine an appropriate value of  $T$ , the natural period of oscillation for our system. When the network is homogeneous,  $T$  from steps 1 and 2 can simply be taken as the natural frequency of each oscillator. In this case, however, we assume that we do not have *a priori* knowledge of  $T$  for the heterogeneous population, and implement steps 1 and 2 by continuously recording  $\bar{s}(\theta)$ , and intermittently perturb the system with  $\delta$ -function pulses. We then take  $T$  to be the period corresponding to the largest mode of the Fourier transformed data  $\bar{s}(\theta)$ , taken over the entire duration of the simulation. By recording the time at which the pulses were presented, we can then extract the portions of the measurement  $\bar{s}(t)$  necessary to implement the numerical procedure. We illustrate this strategy for both a noiseless and uncoupled ( $D = 0$ ,  $\alpha_c = 0$ ) and a noisy and coupled network ( $D = 2$ ,  $\alpha_c = 0.1$ ), with results shown in panels A-C and D-F of Figure 3, respectively. In the noiseless, uncoupled simulations, we take  $q = 1$  to estimate the first Fourier mode of the individual phase response curves, and in Panel C we see that the result agrees well with the average effective PRC of the population. For the network with both noise and coupling, we find in panel F that the magnitude

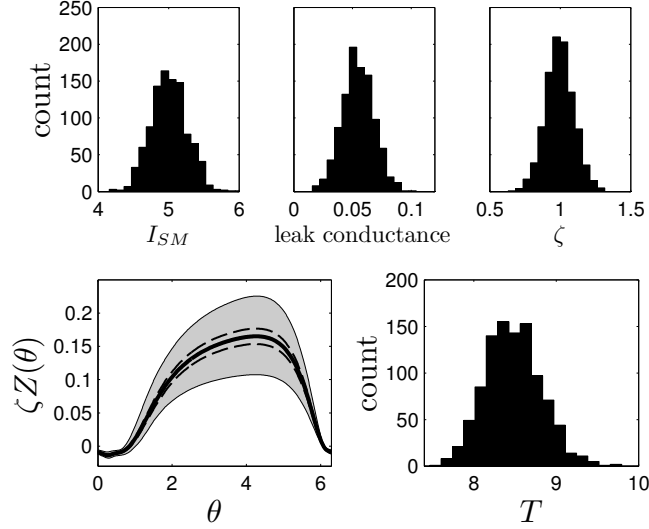


FIG. 2. The top panels show histograms representing the number of neurons with each value of baseline current ( $I_{SM}$ ), leak current conductance, and relative stimulus magnitude,  $\zeta$ , applied to each neuron. The bottom left panel shows the spread of  $\zeta_i Z_i(\theta)$  which represents the effective PRC for each neuron. The boundaries of the shaded region represent maximum and minimum resulting values, the dashed lines represent boundaries of the 25<sup>th</sup> and 75<sup>th</sup> percentiles, and the thick black line gives the average value for the 1000 neuron population. A histogram representing the natural periods of oscillation for each neuron is shown in the bottom-right panel.

and phase of the first Fourier mode are slightly worse than the result from the noiseless, uncoupled network, but the estimate is still quite good. We note that in both examples, the raw phase data from panels B and E do not come close to matching the shape or the magnitude of the individual phase response curves.

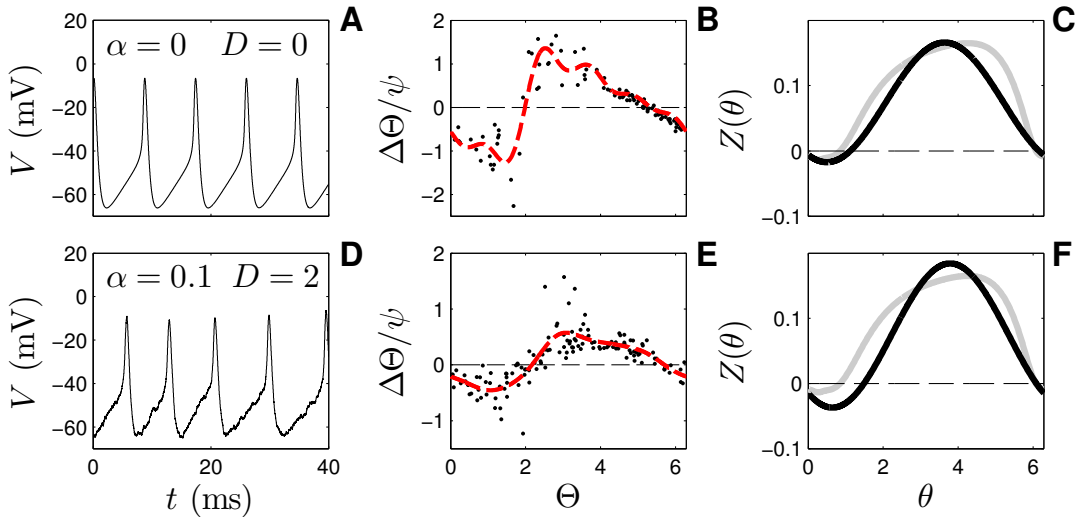


FIG. 3. (Color Online) Panels A-C show results for a population of heterogeneous, uncoupled, noiseless neurons. Panels D-F show results for a population of heterogeneous, coupled, noisy neurons. Panels A and D show an individual neural trace from each population. Panels B and E show the raw data using  $\psi = 1$  as black dots ( $p = 105$  and  $p = 137$  measurements, respectively) while the red line gives a five mode Fourier fit of the raw data. Panels C and F show the resulting PRCs (black lines) and the averaged effective PRC (grey line) for reference.

#### IV. CHOOSING A SIGNAL FOR ROBUST MEASUREMENT OF PRCs

The signal  $s(\theta)$  which each oscillator contributes to the population observation is necessary for determining the distribution before and after the application of the pulsatile stimulus and hence, for finding the PRC. For experimental applications, it is likely that  $s(\theta)$  cannot be obtained with absolute certainty. In this section, we show that PRCs can still be obtained rather robustly if an approximation to the true value of  $s(\theta)$  is known. To begin, consider the infinite time average of (3)

$$\lim_{T \rightarrow \infty} \frac{1}{T} \int_0^T \bar{s}(t) dt = \lim_{T \rightarrow \infty} \frac{1}{T} \int_0^T \left[ \frac{1}{N} \sum_{i=1}^N s(\theta_i(t)) \right] dt. \quad (20)$$

We assume that external perturbations are small so that  $\theta_i(t)$  is well approximated by  $\theta_i(0) + \omega_i t$ . We may then manipulate (20) as follows:

$$\begin{aligned} \lim_{T \rightarrow \infty} \frac{1}{T} \int_0^T \bar{s}(t) dt &= \lim_{T \rightarrow \infty} \left( \frac{1}{T} \int_0^T \left[ \frac{1}{N} \sum_{i=1}^N s(\theta_i(0) + \omega_i t) \right] dt \right), \\ &= \frac{1}{N} \sum_{i=1}^N \lim_{T \rightarrow \infty} \left( \frac{1}{T} \int_0^T \left[ s(\theta_i(0) + \omega_i t) \right] dt \right), \\ &= \frac{1}{2\pi} \int_0^{2\pi} s(\theta) d\theta \left( \frac{1}{N} \sum_{i=1}^N 1 \right), \\ &= \frac{1}{2\pi} \int_0^{2\pi} s(\theta) d\theta. \end{aligned} \quad (21)$$

Therefore, when choosing the signal  $s(\theta)$ , its mean is well approximated by  $\bar{s}(t)$ , provided a long enough measurement is taken. Therefore, it is only necessary to estimate the shape and magnitude of the signal  $s(\theta)$ , as the mean can be determined from the experimental data. Figure 4 replicates the results from Section III using the homogeneous network and the heterogeneous, noisy, coupled network for two different choices of  $s(\theta)$ . For the first choice, we take  $s(\theta)$  to be the true transmembrane voltage, to which we add a Wiener process. The second choice is a simple piecewise linear approximation to an action potential. For both signals, we vertically shift the resulting  $s(\theta)$  so that (21) is satisfied. As long as  $s(\theta)$  is reasonably close to the true signal,  $s^*(\theta)$ , the PRC calculation results are not significantly degraded.

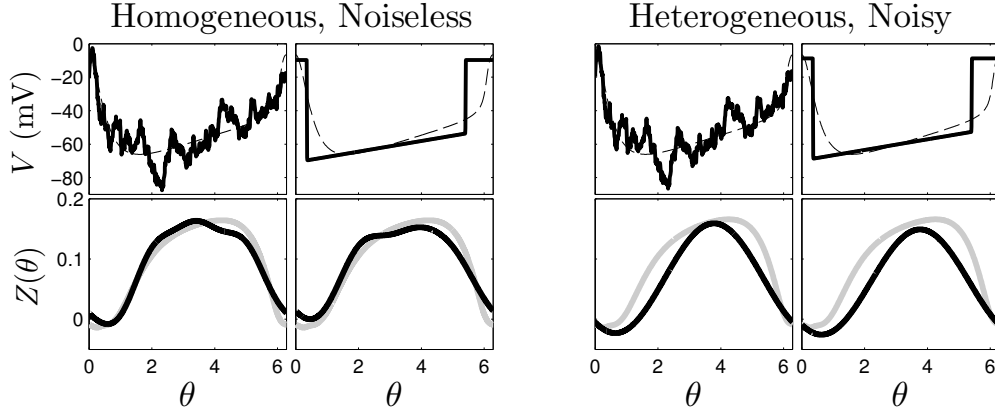


FIG. 4. Left (resp. Right): Replicating the PRC calculation results using the noiseless, homogeneous, uncoupled, (resp. noisy, heterogeneous, coupled) network from Section III using different values of  $s(\theta)$ . Top panels show two different choices of  $s(\theta)$  as bold lines with the true (resp. population average)  $s^*(\theta)$  shown as a dashed line. Bottom panels show the calculated PRCs in black using the  $s(\theta)$  function directly above. Grey lines represent the true (resp. population average) PRC.

## V. BURSTING NEURON PRCs

For a second test, we consider a more complex network of 400 bursting Hindmarsh-Rose model [30] neurons which was modified in [31] to include a synaptic current:

$$\begin{aligned}
 \dot{V}_i &= n_i - aV_i^3 + bV_i^2 - h_i + I \\
 &\quad + \epsilon_{\text{syn}} \sum_{j=1}^N \xi_j (V_i - V_{\text{syn}}) + \epsilon_{\eta} \eta_i(t) + u(t), \\
 \dot{n}_i &= c - dV_i^2 - n_i(t), \\
 \dot{h}_i &= r(\sigma(V_i - V_0) - h_i), \\
 \dot{\xi}_i &= \alpha_{\text{syn}} T_{\infty}(V_i)(1 - \xi_i) - \beta_{\text{syn}} \xi_i, \quad i = 1, \dots, 400.
 \end{aligned} \tag{22}$$

Here,  $V_i$ ,  $n_i$ , and  $h_i$  represent transmembrane voltage and gating variables,  $\xi_i$  is a synaptic variable which could represent a neurotransmitter,  $\eta_i(t) = \mathcal{N}(0, 1)$  is i.i.d. noise with zero mean and variance 1, and  $u(t)$  is an external input. We take  $\epsilon_{\text{syn}} = 0.03$ ,  $\epsilon_{\eta} = 0.01$  and all other parameters identical to those in [31] except for  $\beta_{\text{syn}} = 0.0304$  and  $\alpha_{\text{syn}} = 1.304$  which were modified so that the synaptic variable  $\xi(\theta)$  changed on a slower time scale as compared to the transmembrane voltage  $V(\theta)$ . For this choice of parameters, in the absence of synaptic coupling and noise, each neuron settles to a limit cycle with a period of  $T = 430$  ms consisting of nine-spike bursts followed by a period of quiescence. Here, we use pulses of  $u(t) = 0.4$  for 5 ms so that  $\psi = 2$ . We take  $s(\theta)$  to be the synaptic variable, which is shown in Panel A of Figure 5, but note that similar results can also be achieved by using the transmembrane voltage. Panel B shows  $\bar{s}(t)$  for one of  $p = 106$  measurements, centered about  $t = \tau$ . We note that because of the small noise and coupling terms,  $\bar{s}(t)$  is not perfectly  $T$ -periodic for  $t \neq \tau$ . Panel C shows a fit of five Fourier modes to raw data of  $\Delta\Theta/\psi$  plotted as a function of  $\Theta$ . In panel D, the true PRC calculated using the direct method [3] on a single neuron is shown in grey, and the PRC estimated from the methodology above with  $M = 1000$  and  $q = 5$  is shown in black. The structure of the true PRC is much more complex than in the previous model, but the estimated PRC accurately captures the slowly varying part. To capture the rapid fluctuations in the earlier part of the cycle, we would need to include more Fourier modes in the calculation, but because of noise and network coupling structure, it is not possible to accurately calculate these modes for this model. In panel E, we show that the calculated PRC (black) is very close to the first five Fourier modes of the true PRC (grey). The fit from panel C (red) is also shown for comparison and is not a good approximation of the true PRC.

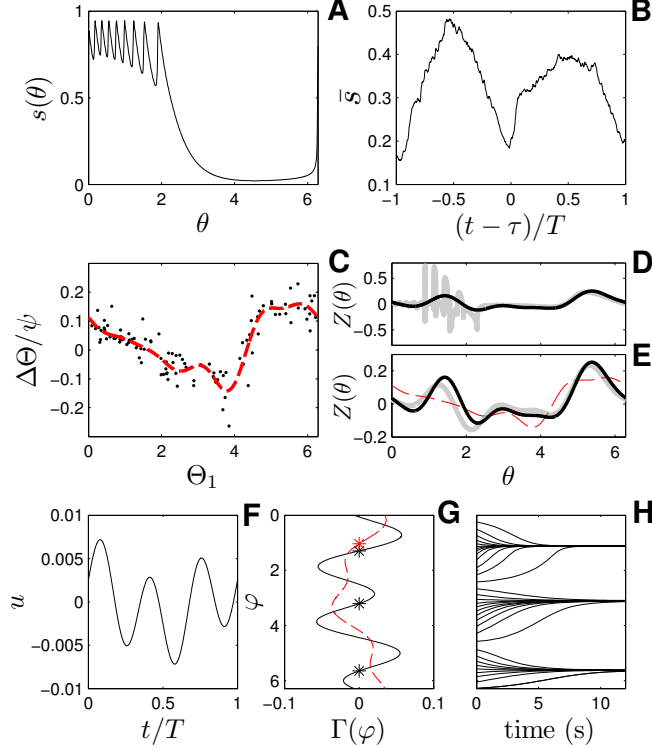


FIG. 5. (Color Online) Panel A shows the synaptic variable,  $\xi$ , as a function of  $\theta$ , which we take to be  $s(\theta)$  in (22). Panel B shows an example measurement of  $\bar{s}$  for a perturbation at  $t = \tau$ . Panel C shows raw data of  $\Delta\Theta/\psi$  plotted against  $\Theta$  with a five mode Fourier fit to the data in red. In panel D, The true PRC is shown in grey with the PRC calculated from the data using  $q = 5$  in black. Panel E shows the first five Fourier modes of the true PRC, the calculated PRC, and the fit from the raw data in grey, black, and red, respectively. We predict the entrainment of (22) to the signal  $u(t)$  shown in panel F. In panel G,  $\Gamma(\varphi)$  is calculated using the red and black curves from panel E, with resulting functions shown in red and black, respectively. Predicted stable fixed points are denoted with \*'s for each curve. The stable fixed points predicted from the black curve accurately predict entrainment as verified from simulations of individual cells from (22) in panel H.

While we cannot calculate the higher order modes which give rise to the rapidly varying part of the PRC, these are not necessary in many applications. In one such example, we use the calculated PRC to predict entrainment of individual neurons from (22) to the external stimulus  $u(t) = 0.0025 \cos(\omega_o t) + 0.005 \sin(\omega_o t)$ , where  $\omega_o = 2\pi/T$ , shown in panel F. If we assume that  $u(t)$  is small enough so that  $\theta(t) \approx \theta(0) + \omega_o t$ , using standard averaging techniques [32], we can reduce the dynamics of individual cells from (22) to

$$\dot{\varphi} = \Gamma(\varphi), \quad (23)$$

where  $\varphi \equiv \theta/\omega_o - t \pmod{T}$  and  $\Gamma(\varphi) = \frac{1}{T} \int_0^T Z(\omega_o t + \varphi) u(t) dt$ . Panel G shows  $\Gamma(\varphi)$  calculated using the PRC obtained from the methodology described in Section II as a black line, which predicts three stable fixed points of (23) marked by \*'s. These fixed points are verified in panel H from numerical simulations of individual, noiseless neurons from (22). For comparison, using the red curve from panel C to calculate  $\Gamma(\varphi)$  predicts only one stable fixed point.

## VI. CONCLUSIONS

This study provides an experimentally feasible methodology for calculating PRCs of individual components from aggregate population data. We have applied this methodology to a model of both periodically spiking

and bursting neurons and show that it can accurately calculate the slowly varying modes of the PRCs in the constituent elements. We explicitly show in Appendix B that in the limit as the truncated order  $\epsilon$  terms from (4) are small, the Fourier coefficients are also accurate to leading order  $\epsilon$ . Nevertheless, when noise and coupling in the system is relatively large, we can still obtain accurate results. Furthermore, using techniques based solely on the direct method [3], as is typically used to measure PRCs, can yield potentially misleading results in the examples presented here.

In each of the examples given here, we are only able to calculate the first few modes of the individual PRCs before either noise, heterogeneity or truncated order  $\epsilon$  effects from the phase reduction begin to significantly degrade the calculation. We do not provide analytical limits on the number of modes we can take, but heuristically we find that as we continue to take more and more modes, the solution becomes dominated by the higher order modes (i.e. the methodology produces PRCs that oscillate rapidly). In a setting where the individual phase PRCs are unknown, the procedure could be repeated for increasing values of  $q$  (yielding solutions with different numbers of Fourier modes) until the higher order Fourier begin to dominate the solution, indicating that the results are no longer valid.

The proposed methodology is shown to work well for the systems tested here, but modifications could improve the accuracy of the calculation. For example, we have chosen a Fourier basis functions to calculate the probability distribution and PRC in (16) because of the intrinsic periodicity of the solutions, and the effect of using different bases has not been investigated here. Furthermore, for simplicity of implementation, we have used a least-square fitting technique to determine the Fourier coefficients, and have not investigated the effect of using different curve fitting techniques. When we considered heterogeneity, coupling and noise in the periodically spiking population of neurons, we were still able to obtain a reasonably accurate estimate of the average phase response curve of the system. It may be possible to improve this estimate by explicitly accounting for these effects in the underlying partial differential equation (4). Most likely this would require specific estimates of the underlying coupling structure and noise strength.

It may be interesting to adapt the proposed methodology for use in excitable systems which through coupling may admit stable periodic oscillations [22]. The constituent elements of these populations are excitable, not periodic, so that perturbations to the individual elements can be understood in terms of isostable response curves [33]. Such systems have relevance to problems in cardiology [34], [35], [36], [37], systems of chemical oscillators [38], waves of spreading depression in the brain [39], [40]. It is possible that isostable response curves could be calculated using a similar strategies for these excitable systems.

Phase reduction has a rich history in the nonlinear sciences, and has led to a greater understanding of many physical, chemical, and biological systems. The methodology presented here could allow for the use of phase reduction in large systems where it is not feasible to directly observe the individual elements, allowing for their study in a more useful coordinate system. In addition, the algorithm presented here is relatively simple and can be readily implemented with modern mathematical software.

Support for this work by National Science Foundation Grant NSF-1264535 is gratefully acknowledged.

## Appendix A: Phase Response Functionals of the Advection Equation

Consider the advection equation, which might describe the probability density  $\rho(t, \theta)$  of a large group of identical phase oscillators, each with phase  $\theta \in [0, 2\pi)$ , on a one dimensional ring, c.f [26]:

$$\frac{\partial \rho}{\partial t} = -\omega \frac{\partial \rho}{\partial \theta} + P(t, \theta). \quad (\text{A1})$$

Here,  $\omega$  is the natural frequency of each oscillator so that the natural period  $T = 2\pi/\omega$  and  $P(t, \theta)$  is a time and phase dependent perturbation. When  $P \equiv 0$ , equation (A1) has a  $T$ -periodic traveling wave solution

$$\rho(t, \theta) = \rho_o(\theta - \omega t), \quad (\text{A2})$$

where  $\rho_o = \rho(0, \theta)$ . In the analysis to follow, we will define this periodic solution as  $\gamma$ .

It will be useful to define a group phase,  $\Theta$ , such that when  $P \equiv 0$ ,  $d\Theta/dt = \omega$ . To this end, we define

$\Theta \in [0, 2\pi)$  as

$$\begin{aligned}\Theta(\rho(t, \theta)) &= \arctan2(a, b), \\ a(t) &= \frac{1}{\pi} \int_0^{2\pi} \rho(t, \theta) \sin \theta d\theta, \\ b(t) &= \frac{1}{\pi} \int_0^{2\pi} \rho(t, \theta) \cos \theta d\theta,\end{aligned}\tag{A3}$$

where  $\arctan2$  is the signed arctangent function, so that the first Fourier mode of the distribution  $\rho(t, \theta)$  is given by  $\sqrt{a^2 + b^2} \cos(\theta - \Theta)$ . Notice that this definition of the group phase allows us to not only define phase in relation to the traveling wave solution,  $\gamma$ , but also for any perturbed solution of (A1).

Changing to group phase coordinates using the chain rule, we find

$$\begin{aligned}\frac{d\Theta}{dt} &= \left\langle \nabla\Theta(\rho), -\omega \frac{\partial\rho}{\partial\theta} + P(t, \theta) \right\rangle \\ &= \omega + \langle \nabla\Theta(\rho), P(t, \theta) \rangle.\end{aligned}\tag{A4}$$

Here,  $\nabla\Theta$  is the group phase response functional (GPRF) which represents the gradient of the group phase field and  $\langle \cdot, \cdot \rangle$  is the  $L^2$  inner product. Note that equivalence in (A4) comes from the fact that  $d\Theta/dt = \omega$  when  $P \equiv 0$ . In order to use (A4) we need an explicit expression for the GPRF. Following a similar derivation of an adjoint equation for the calculation of GPRFs for limit cycle oscillators [22], evaluating the vector field at  $\rho^\gamma(\Theta)$  which we define as the intersection of the  $\Theta$  level set and the trajectory  $\gamma$ , we have

$$\frac{d\Theta}{dt} = \omega + \langle \nabla\Theta(\rho^\gamma(\Theta)), P(t, \theta) \rangle.\tag{A5}$$

To proceed, we assume that  $P \equiv 0$  for  $t > 0$  and give a small perturbation  $\Delta\rho$  at time  $t = 0$  to the trajectory  $\rho(t, \theta) \in \gamma$ . Letting  $\rho_\epsilon(t, \theta) = \rho^\gamma(t, \theta) + \Delta\rho(t, \theta)$  be the perturbed initial condition, we have

$$\begin{aligned}\frac{\partial\Delta\rho(t, \theta)}{\partial t} &= J(\rho(t, \theta)) \cdot \Delta\rho(t, \theta) + \mathcal{O}(\|\Delta\rho(t, \theta)\|^2) \\ &= -\omega \frac{\partial}{\partial\theta} \cdot \Delta\rho(t, \theta) + \mathcal{O}(\|\Delta\rho(t, \theta)\|^2),\end{aligned}\tag{A6}$$

where  $J \equiv -\omega \frac{\partial}{\partial\theta}$ . We also define the phase shift associated with the perturbation  $\Delta\rho(t, \theta)$  as  $\Delta\Theta = \Theta(\rho_\epsilon(t, \theta)) - \Theta(\rho(t, \theta))$  and write

$$\Delta\Theta = \langle \nabla_{\rho(t, \theta)}\Theta, \Delta\rho(t, \theta) \rangle + \mathcal{O}(\|\Delta\rho(t, \theta)\|^2),\tag{A7}$$

where  $\nabla_{\rho(t, \theta)}\Theta$  is the gradient of  $\Theta$  evaluated at  $\rho(t, \theta)$ . After the initial perturbation at  $t = 0$ ,  $\Delta\Theta$  is independent of time, and taking time derivatives of (A7) and neglecting  $\mathcal{O}(\|\Delta\rho(t, \theta)\|^2)$  terms gives

$$\begin{aligned}\left\langle \frac{\partial\nabla_{\rho(t, \theta)}\Theta}{\partial t}, \Delta\rho(t, \theta) \right\rangle &= - \left\langle \nabla_{\rho(t, \theta)}\Theta, \frac{\partial\Delta\rho(t, \theta)}{\partial t} \right\rangle \\ &= - \left\langle \nabla_{\rho(t, \theta)}\Theta, -\omega \frac{\partial}{\partial\theta} \cdot \Delta\rho(t, \theta) \right\rangle \\ &= - \left\langle \omega \frac{\partial}{\partial\theta} \cdot \nabla_{\rho(t, \theta)}\Theta, \Delta\rho(t, \theta) \right\rangle.\end{aligned}\tag{A8}$$

Equivalence in the last line comes from the fact that  $\omega \frac{\partial}{\partial\theta}$  is the adjoint of  $-\omega \frac{\partial}{\partial\theta}$  on the periodic domain. Equation (A8) holds for arbitrary perturbation  $\Delta\rho(t, \theta)$  and therefore gives the relation

$$\frac{\partial\nabla_{\rho(t, \theta)}\Theta}{\partial t} = -\omega \frac{\partial}{\partial\theta} \cdot \nabla_{\rho(t, \theta)}\Theta.\tag{A9}$$

Equations of the form (A9) are sometimes referred to as ‘‘adjoint equations’’ for calculating phase response functionals (or phase response curves) [22], [6]. The GPRF for this system will be a  $T$ -periodic solution to

(A9) which also satisfies  $\langle \nabla_{\rho(t,\theta)} \Theta, -\omega \partial \rho / \partial \theta \rangle = \omega$ , as was required by (A4). Furthermore, because the phase  $\Theta$  was defined to be a function of the first Fourier mode of the distribution  $\rho$ , any perturbations to higher modes will not effect the group phase. Therefore,

$$\langle \nabla_{\rho(t,\theta)} \Theta, p \sin(n\theta) + q \cos(n\theta) \rangle = 0, \quad \forall p, q \in \mathbb{R}, \quad \forall n = 2, 3, 4, \dots, \quad (\text{A10})$$

which means that the GPRF must be of the form

$$\nabla_{\rho(t,\theta)} \Theta = \alpha \sin(\theta - \vartheta), \quad (\text{A11})$$

with  $\alpha \in \mathbb{R}$  and  $\vartheta \in [0, 2\pi)$ . Recalling that when  $P \equiv 0$ ,  $d\Theta/dt = \omega$ , one can verify that for the group phase defined in (A3), the GPRF is given by

$$\nabla_{\rho(t,\theta)} \Theta = \frac{\sin(\theta - \Theta)}{\pi \sqrt{a^2 + b^2}}. \quad (\text{A12})$$

## Appendix B: Measuring Phase Response Curves in an Almost Advective Equation

Here, we will show that using the methodology presented in the main text to estimate phase response curves,  $Z(\theta)$ , will yield results that are accurate to leading order  $\epsilon$  regardless of whether the true dynamics evolve according to

$$\frac{\partial \rho}{\partial t} = -\omega \rho_\theta - [Z(\theta) \rho_\theta + Z_\theta \rho] \psi \delta(t - \tau) \quad (\text{B1})$$

or

$$\frac{\partial \rho}{\partial t} = -\omega \rho_\theta - [Z(\theta) \rho_\theta + Z_\theta \rho] \psi \delta(t - \tau) + \mathcal{O}(\epsilon), \quad (\text{B2})$$

where the  $\mathcal{O}(\epsilon)$  terms represent small but unknown perturbations. In the main text, all results are obtained using (B1), and those results will be used for comparison here.

To begin, in the presence of the  $\mathcal{O}(\epsilon)$  terms, suppose that at  $t = \tau - T$  the probability distribution is  $\rho_o(\theta)$ . Using the asymptotic expansion (5) from Section II A of the main text, at time  $t = \tau^-$  the solution of (B2) will be

$$\rho(\tau^-, \theta) = \rho_o(\theta) + \epsilon \int_{\tau-T}^{\tau} [\rho^{(1)}(t, \theta) + \mathcal{O}(\epsilon)] dt. \quad (\text{B3})$$

Therefore,  $\rho(\tau^-, \theta) = \rho_o(\theta) + \mathcal{O}(\epsilon)$ . To calculate  $G(\theta, \Theta_1)$ , where  $\Theta_1 \equiv \Theta(\tau^-)$ , we need to know  $\Theta(\tau^-)$ , which can be found by calculating Fourier coefficients of (B3):

$$\begin{aligned} a &= \frac{1}{\pi} \int_0^{2\pi} \rho_o(\theta) \sin(\theta) d\theta + \frac{\epsilon}{\pi} \int_0^{2\pi} \left\{ \int_{\tau-T}^{\tau} [\rho^{(1)}(t, \theta) + \mathcal{O}(\epsilon)] dt \right\} \sin(\theta) d\theta = a^* + \mathcal{O}(\epsilon), \\ b &= \frac{1}{\pi} \int_0^{2\pi} \rho_o(\theta) \cos(\theta) d\theta + \frac{\epsilon}{\pi} \int_0^{2\pi} \left\{ \int_{\tau-T}^{\tau} [\rho^{(1)}(t, \theta) + \mathcal{O}(\epsilon)] dt \right\} \cos(\theta) d\theta = b^* + \mathcal{O}(\epsilon), \end{aligned} \quad (\text{B4})$$

where  $a^*$  and  $b^*$  are the Fourier coefficients if we were using (B1). Therefore, the group phase is  $\Theta_1 = \arctan 2(a^* + \mathcal{O}(\epsilon), b^* + \mathcal{O}(\epsilon))$  which through Taylor expansion can be shown to be equal to  $\arctan 2(a^*, b^*) + \mathcal{O}(\epsilon) = \Theta_1^* + \mathcal{O}(\epsilon)$ , where  $\Theta_1^*$  would be the group phase if we were using (B1). Then from (A12),

$$G(\theta, \Theta_1) = \frac{\sin(\theta - \Theta_1^* + \mathcal{O}(\epsilon))}{\pi \sqrt{a^{*2} + b^{*2} + \mathcal{O}(\epsilon)}} = \frac{\sin(\theta - \Theta_1^*)}{\pi \sqrt{a^{*2} + b^{*2}}} + \mathcal{O}(\epsilon). \quad (\text{B5})$$

Note that equivalence in (B5) comes from Taylor expansion and assumes that  $\sqrt{a^{*2} + b^{*2}}$  is large compared to  $\epsilon$ . Using the phase reduction for (B2), the effect on the  $\delta$ -function pulse on the group phase will be

$$\begin{aligned} \Delta \Theta &= -\frac{\psi}{\pi \sqrt{a^{*2} + b^{*2}}} \left\langle \sin(\theta - \Theta_1^*) + \mathcal{O}(\epsilon), \frac{\partial}{\partial \theta} (\rho_o(\theta) + \epsilon \rho^{(1)}(\tau^-, \theta) + \mathcal{O}(\epsilon^2)) Z(\theta) \right. \\ &\quad \left. + \frac{\partial}{\partial \theta} Z(\theta) (\rho_o(\theta) + \epsilon \rho^{(1)}(\tau^-, \theta) + \mathcal{O}(\epsilon^2)) \right\rangle \\ \implies \Delta \Theta + \mathcal{O}(\epsilon) &= -\frac{\psi}{\pi \sqrt{a^{*2} + b^{*2}}} \langle \sin(\theta - \Theta_1^*), \rho_o'(\theta) Z(\theta) + Z'(\theta) \rho_o(\theta) \rangle, \end{aligned} \quad (\text{B6})$$

where  $' \equiv \partial/\partial\theta$ . Note that equivalence in the last line of (B6) requires that the derivatives of the  $\mathcal{O}(\epsilon)$  terms are still  $\mathcal{O}(\epsilon)$ . We observe that the right hand side of (B6) is of the same form as (15) from the main text. Therefore, including the  $\mathcal{O}(\epsilon)$  terms from (B2) will cause the effect of the  $\delta$ -function pulse to differ by  $\mathcal{O}(\epsilon)$ .

In Section II A from the main text, we show that to leading order  $\epsilon$ , we can measure the phase of a distribution that evolves according to (B2) by measuring  $\bar{s}(t)$  for one period. Therefore, for an initial distribution  $\rho(\tau - T, \theta)$ , if we apply the methodology from the main text to measure the phase response curve of the system,

$$\Theta_1 = \Theta_1^* + \mathcal{O}(\epsilon). \quad (\text{B7})$$

Using the coefficients from (B4) the true value of the group phase at  $\tau^-$ ,  $\tilde{\Theta}(\tau^-)$ , is equal to  $\Theta_1^* + \mathcal{O}(\epsilon)$ , and using (B6) we can say that after the pulse  $\tilde{\Theta}(\tau^+) = \Theta_1^* + \Delta\Theta^* + \mathcal{O}(\epsilon)$ , where  $\Delta\Theta^*$  is the change in group phase if the distribution evolved according to (B1). Again, we will be able to measure the group phase of  $\rho(\tau^+, \theta)$  to leading order  $\epsilon$ , so that

$$\Theta_2 = \Theta_1^* + \Delta\Theta^* + \mathcal{O}(\epsilon) \quad (\text{B8})$$

and

$$\Delta\Theta = \Theta_2 - \Theta_1 = \Delta\Theta^* + \mathcal{O}(\epsilon). \quad (\text{B9})$$

Therefore,  $b = b^* + \mathcal{O}(\epsilon)$ , where  $b$  is a vector of readings of  $\Delta\Theta$ , and  $b^*$  is what would have been measured if the distribution evolved according to (B1).

We now turn our attention to the values in the  $A$  matrix given by (18) from the main text. In equation (13) from Section II B from the main text, we show that we can calculate the Fourier coefficients of  $\rho_o$  to leading order in  $\epsilon$ . Therefore, the truncated distribution from equation (16) of the main text can be written as

$$\begin{aligned} \rho_f(\theta) &= \rho_o(\theta) - \sum_{k=q+1}^{\infty} B_{\rho,k} \sin(k(\phi_\rho - \theta)) + \mathcal{O}(\epsilon) \\ &= \rho_f^*(\theta) + \mathcal{O}(\epsilon), \end{aligned} \quad (\text{B10})$$

where  $B_{\rho,k} \sin(k(\phi_\rho - \theta))$  is the  $k^{\text{th}}$  Fourier mode of  $\rho_o(\theta)$  and  $\rho_f^*(\theta)$  is the function  $\rho_f(\theta)$  that would have been calculated if the probability distribution evolved according to (B1). Therefore, the values in  $A$  calculated from equation (18) from the main text become

$$\begin{aligned} A_{k,1} &= -\psi \langle G(\theta, \Theta^*) + \mathcal{O}(\epsilon), (\rho_{f,k}^* + \mathcal{O}(\epsilon))' \rangle = A_{k,1}^* + \mathcal{O}(\epsilon) \\ A_{k,2v} &= -\psi \langle G(\theta, \Theta^*) + \mathcal{O}(\epsilon), \sin(v\theta)(\rho_{f,k}^* + \mathcal{O}(\epsilon))' + v \cos(v\theta)(\rho_{f,k}^* + \mathcal{O}(\epsilon)) \rangle = A_{k,2v}^* + \mathcal{O}(\epsilon) \\ A_{k,2w+1} &= -\psi \langle G(\theta, \Theta^*) + \mathcal{O}(\epsilon), \cos(w\theta)(\rho_{f,k}^* + \mathcal{O}(\epsilon))' - w \sin(w\theta)(\rho_{f,k}^* + \mathcal{O}(\epsilon)) \rangle = A_{k,2w+1}^* + \mathcal{O}(\epsilon), \end{aligned} \quad (\text{B11})$$

where  $A_{i,j}^*$  is the value of  $A_{i,j}$  that would have been calculated if the probability distribution evolved according to (B1). Therefore, to calculate the Fourier coefficients  $c$  of  $Z(\theta)$  we must solve

$$(A^* + \epsilon E)c = b^* + \epsilon\beta \quad (\text{B12})$$

so that  $c = (A^* + \epsilon E)^\dagger b^* + \epsilon(A^* + \epsilon E)^\dagger \beta$ . Here,  $\epsilon E$  represents the  $\mathcal{O}(\epsilon)$  terms from (B11) and  $\epsilon\beta$  represents the  $\mathcal{O}(\epsilon)$  terms from (B9).

Consider the difference between  $c$  and  $c^* = A^{*\dagger} b^*$ , and let  $D = (A^* + \epsilon E)$ . Then

$$\begin{aligned} c - c^* &= D^\dagger b^* + \epsilon D^\dagger \beta - A^{*\dagger} b^* \\ \|c - c^*\| &= \|(D^\dagger - A^{*\dagger})b^* + \epsilon D^\dagger \beta - \epsilon A^{*\dagger} \beta + \epsilon A^{*\dagger} \beta\| \\ &= \|(D^\dagger - A^{*\dagger})(b^* + \epsilon\beta) + \epsilon A^{*\dagger} \beta\| \\ &\leq \|D^\dagger - A^{*\dagger}\| \cdot \|b^* + \epsilon\beta\| + \epsilon \|A^{*\dagger}\| \cdot \|\beta\|. \end{aligned} \quad (\text{B13})$$

Because the difference between the true Fourier coefficients and  $c^*$  is  $\mathcal{O}(\epsilon)$ , if we can show that  $\|D^\dagger - A^{*\dagger}\|$  is an order  $\epsilon$  term, then the difference between  $c$  and the true Fourier coefficients will also be  $\mathcal{O}(\epsilon)$ .

To proceed, we assume that we have taken enough independent measurements of  $\Delta\Theta$  so that  $A^*$  has full rank. Then, let  $U\Sigma V^T$  be the singular value decomposition of  $A$  so that

$$\Sigma = \begin{bmatrix} \Sigma_{11} \\ 0 \end{bmatrix}, \quad U^T E V = \begin{bmatrix} E_{11} \\ E_{21} \end{bmatrix}, \quad U^T D V = \begin{bmatrix} D_{11} \\ D_{21} \end{bmatrix} = \begin{bmatrix} \Sigma_{11} + \epsilon E_{11} \\ \epsilon E_{21} \end{bmatrix}. \quad (\text{B14})$$

Using a combination of Theorem 2.2 and Theorem 3.8 from [41], if we assume  $\epsilon E$  is small enough so that it is an acute perturbation of  $A^*$ , as defined in [41], we can write

$$\|D^\dagger - A^{*\dagger}\| \leq \frac{\epsilon \|\Sigma_{11}^{-1}\|_2 \|A^{*\dagger}\| (\|E_{11}\| + \|E_{21}\|)}{1 - \epsilon \|E_{11}\|_2 \|\Sigma_{11}^{-1}\|_2}. \quad (\text{B15})$$

Therefore,  $\|D^\dagger - A^{*\dagger}\|$  can be bounded as an  $\mathcal{O}(\epsilon)$  term, and from (B13),  $c$  is at most  $\mathcal{O}(\epsilon)$  away from  $c^*$  which is in turn  $\mathcal{O}(\epsilon)$  away from the true Fourier coefficients of  $Z(\theta)$ .

- 
- [1] A. Winfree. *The Geometry of Biological Time*. Springer Verlag, New York, 2nd edition, 2001.
  - [2] Y. Kuramoto. *Chemical Oscillations, Waves, and Turbulence*. Springer-Verlag, Berlin, 1984.
  - [3] E. M. Izhikevich. *Dynamical Systems in Neuroscience: The Geometry of Excitability and Bursting*. MIT Press, London, 2007.
  - [4] F. C. Hoppensteadt and E. M. Izhikevich. *Weakly Connected Neural Networks*. Springer, New York, 1997.
  - [5] G. B. Ermentrout and D. H. Terman. *Mathematical Foundations of Neuroscience*. Springer, New York, 2010.
  - [6] E. Brown, J. Moehlis, and P. Holmes. On the phase reduction and response dynamics of neural oscillator populations. *Neural Computation*, 16(4):673–715, 2004.
  - [7] P. A. Tass. Desynchronization of brain rhythms with soft phase-resetting techniques. *Biological Cybernetics*, 87(2):102–115, 2002.
  - [8] C. Wilson, B. Beverlin II, and T. Netoff. Chaotic desynchronization as the therapeutic mechanism of deep brain stimulation. *Front. Syst. Neurosci.*, 5:Art. No. 50, 2011.
  - [9] D. Wilson, A. B. Holt, T. I. Netoff, and J. Moehlis. Optimal entrainment of heterogeneous noisy neurons. *Frontiers in Neuroscience*, 9:192, 2015.
  - [10] S. An, R. Harang, K. Meeker, D. Granados-Fuentes, C. A. Tsai, C. Mazuski, J. Kim, F. J. Doyle, L. R. Petzold, and E. D. Herzog. A neuropeptide speeds circadian entrainment by reducing intercellular synchrony. *Proceedings of the National Academy of Sciences*, 110(46):E4355–E4361, 2013.
  - [11] N. Bagheri, S. R. Taylor, K. Meeker, L. R. Petzold, and F. J. Doyle. Synchrony and entrainment properties of robust circadian oscillators. *Journal of The Royal Society Interface*, 5(Suppl 1):S17–S28, 2008.
  - [12] G. B. Ermentrout. *Simulating, Analyzing and Animating Dynamical Systems: A Guide to XPPAUT for Researchers and Students*. SIAM, Philadelphia, 2002.
  - [13] W. Govaerts and B. Sautois. Computation of the phase response curve: a direct numerical approach. *Neural Computation*, 18(4):817–847, 2006.
  - [14] A. Dhooge, W. Govaerts, and Y. A. Kuznetsov. MATCONT: a MATLAB package for numerical bifurcation analysis of ODEs. *ACM Transactions on Mathematical Software*, 29(2):141–164, 2003.
  - [15] R. F. Galán, G. B. Ermentrout, and N. N. Urban. Efficient estimation of phase-resetting curves in real neurons and its significance for neural-network modeling. *Physical Review Letters*, 94(15):158101, 2005.
  - [16] T. Netoff, M. A. Schwemmer, and T. J. Lewis. Experimentally estimating phase response curves of neurons: theoretical and practical issues. In *Phase Response Curves in Neuroscience*, pages 95–129. Springer, New York, 2012.
  - [17] G. T. Einevoll, C. Kayser, N. K. Logothetis, and S. Panzeri. Modelling and analysis of local field potentials for studying the function of cortical circuits. *Nature Reviews Neuroscience*, 14(11):770–785, 2013.
  - [18] Y. Kawamura, H. Nakao, K. Arai, H. Kori, and Y. Kuramoto. Collective phase sensitivity. *Physical Review Letters*, 101(2):024101, 2008.
  - [19] Tae-Wook Ko and G Bard Ermentrout. Phase-response curves of coupled oscillators. *Physical Review E*, 79(1):016211, 2009.
  - [20] H. Kori, Y. Kawamura, H. Nakao, K. Arai, and Y. Kuramoto. Collective-phase description of coupled oscillators with general network structure. *Physical Review E*, 80(3):036207, 2009.
  - [21] Z. Levnajić and A. Pikovsky. Phase resetting of collective rhythm in ensembles of oscillators. *Physical Review E*, 82(5):056202, 2010.
  - [22] H. Nakao, T. Yanagita, and Y. Kawamura. Phase-reduction approach to synchronization of spatiotemporal rhythms in reaction-diffusion systems. *Physical Review X*, 4(2):021032, 2014.

- [23] I. Z. Kiss, C. G. Rusin, H. Kori, and J. L. Hudson. Engineering complex dynamical structures: Sequential patterns and desynchronization. *Science*, 316:1886–1889, 2007.
- [24] A. Zlotnik, Y. Chen, I. Z. Kiss, H. A. Tanaka, and J. S. Li. Optimal waveform for fast entrainment of weakly forced nonlinear oscillators. *Physical Review Letters*, 111(2):024102, 2013.
- [25] D. Wilson and J. Moehlis. Optimal chaotic desynchronization for neural populations. *SIAM Journal on Applied Dynamical Systems*, 13(1):276–305, 2014.
- [26] P. A. Tass. *Phase Resetting in Medicine and Biology: Stochastic Modelling and Data Analysis*. Springer, New York, 2007.
- [27] C. D. Meyer. *Matrix Analysis and Applied Linear Algebra*. SIAM, Philadelphia, 2000.
- [28] J. Rubin and D. Terman. High frequency stimulation of the subthalamic nucleus eliminates pathological thalamic rhythmicity in a computational model. *Journal of Computational Neuroscience*, 16:211–235, 2004.
- [29] D. Johnston and S. M.-S. Wu. *Foundations of Cellular Neurophysiology*. MIT Press, Cambridge, MA, 1995.
- [30] J. L. Hindmarsh and R. M. Rose. A model of neuronal bursting using three coupled first order differential equations. *Proceedings of the Royal Society of London. Series B. Biological Sciences*, 221(1222):87–102, 1984.
- [31] E. Sherwood and J. Guckenheimer. Dissecting the phase response of a model bursting neuron. *SIAM Journal on Applied Dynamical Systems*, 9:659–703, 2010.
- [32] J. A. Sanders, F. Verhulst, and J. Murdock. *Averaging Methods in Nonlinear Dynamical Systems*. Springer-Verlag, New York, second edition, 2007.
- [33] D. Wilson and J. Moehlis. Extending phase reduction to excitable media: Theory and applications. *SIAM Review*, 57(2):201–222, 2015.
- [34] E. M. Cherry and F. H. Fenton. Visualization of spiral and scroll waves in simulated and experimental cardiac tissue. *New Journal of Physics*, 10(12):125016, 2008.
- [35] F. Fenton, E. Cherry, H. Hastings, and S. Evans. Multiple mechanisms of spiral wave breakup in a model of cardiac electrical activity. *Chaos*, 12:852–892, 2002.
- [36] Z. Qu, A. Garfinkel, P. Chen, and J. N. Weiss. Mechanisms of discordant alternans and induction of reentry in simulated cardiac tissue. *Circulation*, 102(14):1664–1670, 2000.
- [37] D. J. Christini, M. L. Riccio, C. A. Cuiianu, J. J. Fox, A. Karma, and R. F. Gilmour Jr. Control of electrical alternans in canine cardiac Purkinje fibers. *Physical Review Letters*, 96(10):104101, 2006.
- [38] M. Hildebrand, J. Cui, E. Mihaliuk, J. Wang, and K. Showalter. Synchronization of spatiotemporal patterns in locally coupled excitable media. *Physical Review E*, 68(2):026205, 2003.
- [39] M. Lauritzen, J. P. Dreier, M. Fabricius, J. A. Hartings, R. Graf, and A. J. Strong. Clinical relevance of cortical spreading depression in neurological disorders: migraine, malignant stroke, subarachnoid and intracranial hemorrhage, and traumatic brain injury. *Journal of Cerebral Blood Flow & Metabolism*, 31(1):17–35, 2011.
- [40] A. C. Charles and Serapio M S. M. Baca. Cortical spreading depression and migraine. *Nature Reviews Neurology*, 9(11):637–644, 2013.
- [41] G. W. Stewart. On the perturbation of pseudo-inverses, projections and linear least squares problems. *SIAM Review*, 19(4):634–662, 1977.